Improved State of Health Assessment for Lithium-Ion Batteries Based on Electrochemical Impedance Spectroscopy Measurements

Gabriele Patrizi[1], Fabio Canzanella[1], and Lorenzo Ciani[1]

[1]*Department of Information Engineering, University of Florence, Florence, Via di S. Marta,3, 50139, Italy*

gabriele.patrizi@unifi.it
fabio.canzanella@unifi.it
lorenzo.ciani@unifi.it

ABSTRACT

Conventionally, battery State of Health (SOH) is defined through the measurement of discharge capacity. However, such approaches are poorly suited for online and in-vehicle applications, as they require full charge/discharge cycles and accurate current integration over long periods. For this reason, indirect health indicators are widely adopted, especially in automotive PHM frameworks. In this context, Electrochemical Impedance Spectroscopy (EIS) has proven to be an effective tool for investigating battery degradation, as it provides detailed insight into internal electrochemical processes. Nevertheless, EIS measurements are strongly influenced by the operating conditions of the tested device, which reduces their practical value under high or variable stress levels. To address these limitations, this work proposes a robust procedure to extract a one-dimensional Health Indicator (HI) from EIS measurements performed after the electric vehicle (EV) charge phase. Instead of relying on full-spectrum fitting or equivalent circuit modeling which are often computationally intensive and difficult to implement online, the proposed method extracts multiple physically meaningful geometrical features directly from Nyquist plots. The features are normalized and evaluated through an adaptive selection process that identifies the most informative ones for degradation tracking and prognostics, ensuring robustness under varying stress conditions. The selected features are then combined through an innovative algorithm to generate a single HI that accurately reflects the battery degradation trend, enabling integration into automotive Battery Management Systems (BMS). To ensure generalizability and repeatability, the approach is validated at different processing stages using a custom dataset of lithium-ion cells tested under highly stressful charge and discharge conditions for a total of 400 cycles.

1. INTRODUCTION

Assessing the State of Health (SOH) of lithium-ion batteries is critical to ensure reliable, safe, and long-term operation in automotive applications (Lee et al., 2024). In electric vehicles (EVs), battery degradation directly impacts driving range, safety, and lifecycle cost, making SOH assessment of primary importance (Omakor et al., 2024). The most straightforward definition of SOH is the percentage ratio between the measured discharge capacity and the rated capacity of the cell (Yang et al., 2021). This definition directly associates the battery's health condition with the residual energy it can still deliver. However, obtaining accurate capacity measurements is challenging, as it requires continuous current integration and prior knowledge of the initial battery State of Charge (SOC) (Dini et al., 2024).

These limitations have led researchers to investigate alternative indirect health indicators (HIs). Among indirect techniques, Electrochemical Impedance Spectroscopy (EIS) has emerged as a powerful diagnostic tool, capable of capturing degradation mechanisms such as loss of active material, lithium plating, and increases in internal resistance (Iurilli et al., 2021). By providing frequency-dependent information on internal electrochemical processes, EIS enables a deeper understanding of battery aging.

Figure 1 shows a representative example of Nyquist impedance spectra acquired at different SOH levels. As degradation progresses, a clear rightward shift of the spectrum can be observed, indicating an increase in ohmic resistance. In addition, the enlargement of the semicircular region reflects the growth of charge transfer resistance, while variations in the low-frequency tail suggest changes in diffusion-related phenomena. These systematic modifications confirm that EIS spectra embed physically meaningful information correlated with battery aging, making them suitable candidates for the extraction of robust Health Indicators.

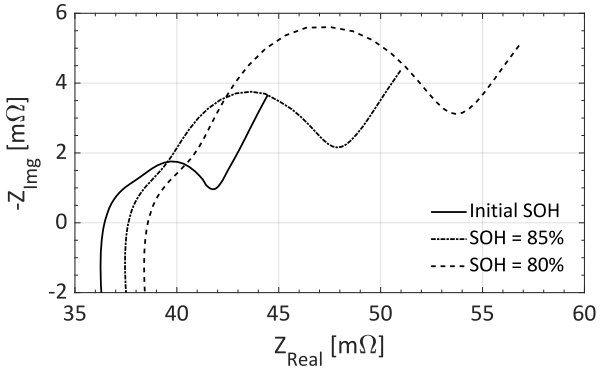

Figure 1. Nyquist plots of the impedance at different SOHs

Consequently, numerous studies have focused on the development of EIS-based HIs. For instance, (Zhou et al., 2023) propose an HI based on geometrical analysis of impedance spectra, identifying a clear correlation between capacity and charge transfer resistance estimated from EIS data. Similarly, (Guo et al., 2024) establish equivalent circuit model parameters for SOH assessment of $LiFePO_4$ batteries. However, these approaches rely on the definition of a reference Equivalent Circuit Model (ECM) which should be accurate while limiting its generalizability to heterogenous battery datasets. Nevertheless, EIS measurements are highly sensitive to operating conditions, including temperature, state of charge, and applied current. In automotive environments, where batteries are subjected to high discharge rates and dynamically varying loads, this sensitivity can significantly limit the robustness and practical applicability of EIS-based indicators (Shan et al., 2025). To address these issues, (Du et al., 2025) present a robust feature selection strategy to enhance EIS-based diagnostics. However, their optimal correlation-based approach fits the impedance data using a Voigt ECM model and then applies XGBoost (eXtreme Gradient Boosting) algorithms, increasing the computational complexity required for practical real-time on-vehicle implementation. A faster algorithm has been proposed by (Dong et al., 2024), which exploits a comprehensive analysis of impedance characteristics to develop an SOH assessment model valid over a wide temperature range. Despite promising performance, this method relies on large datasets from a single battery model, limiting its generalizability. EIS-based prediction can also be improved by integrating additional thermal, temporal, and electrical measurements, as demonstrated in (Patrizi et al., 2025).

In contrast, this paper proposes a novel method to extract a robust single HI using only EIS data without any need to account for a reference ECM. Specifically, 18 features are directly derived from the geometrical characteristics of Nyquist spectra, including the dimensions of semicircles, the value and position of local maxima and minima, the slope of linear regions, and the area under the curve in different frequency ranges. Furthermore, the proposed framework introduces a custom feature score that accounts for each feature's correlation with an expected single-exponential degradation model, while penalizing unstable and noisy features. The selected features are then linearly combined with an additional regularization term derived from an early fitting of the HI to a reference exponential degradation model, improving estimation accuracy. This strategy addresses a critical limitation of multi-feature approaches. While multi-feature techniques can achieve accurate SOH monitoring through Machine Learning algorithms or Neural Networks (Bian et al., 2025), their computational complexity is often unsuitable for direct real-time on-vehicle implementation. Therefore, dimensionality reduction is required to simplify the health estimation problem. Principal Component Analysis (PCA) methods are widely adopted because they effectively reduce dimensionality by prioritizing features with the greatest variance. However, PCA can be sensitive to noise, often requiring additional processing steps with higher computational cost, and it does not explicitly prioritize features whose trends are most suitable for degradation diagnostics (Yu et al., 2024). In contrast, the technique proposed in this work adaptively emphasizes trends that exhibit the highest similarity to the expected degradation curve, introducing a model-guided criterion to improve HI performance.

The proposed methodology is validated on a custom experimental dataset consisting of lithium-ion cells cycled under stressful conditions representative of EV usage. The cells undergo 400 usage cycles, with charging performed using a Constant-Current Constant-Voltage (CCCV) protocol at a 1.6C rate and discharging under constant current at 4C rate. At the end of each charging phase, after appropriate stabilization, EIS measurements are collected over a frequency range from 50 mHz to 50 kHz. The monitoring capability of the proposed method is compared with reference SOH curves derived from actual capacity decay and with HIs obtained through traditional PCA, demonstrating promising improvements in battery SOH assessment. Furthermore, the method is validated through a formal analysis at different processing stages, highlighting the transparency and robustness of this modular technique for online diagnostics and prognostics of Lithium-Ion Batteries.

2. PROPOSED METHODOLOGY

2.1. EIS-based Feature Extraction

The core idea of the proposed framework is to develop a novel and robust one-dimensional HI based exclusively on EIS data. The complete schematic workflow of the methodology is illustrated in Figure 2. The selected features are derived from the low-frequency (LF) and mid-frequency (MF) regions of the spectrum. This choice is motivated by the well-established association of these frequency ranges with charge-transfer and diffusion processes occurring within the cell, which evolve with the number of endured cycles and therefore act as indirect indicators of battery degradation.

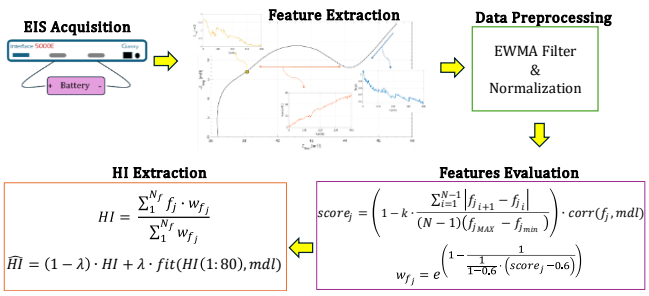

Figure 2. Visual schematic of the proposed framework

An additional criterion in the feature selection process is that all features must be obtainable through straightforward calculations directly from the acquired EIS, without requiring equivalent circuit modeling or complex procedures. The complete list of the features considered is reported below:

1. *Arch height*: distance between the local maximum of the intermediate semicircle and the real axis of the spectrum.
2. *Arch width*: total width of the MF semicircle.
3. *Area LF*: area subtended by the LF region.
4. *Area MF*: area subtended by the MF region.
5. *Average* Z_{img} *:* mean value of the imaginary component of the impedance
6. *Average* Z_{real}*:* mean value of the real component of the impedance.
7. *R0:* ohmic resistance of the battery.
8. *Range* Z_{img}: range of the imaginary component within the examined frequency regions.
9. *Range* Z_{real}: range of the real component within the examined frequency regions.
10. *Warburg Linearity:* R^2 value of a linear fit applied to the LF region.
11. *Warburg Slope:* slope of the linear trend observed in the LF region.
12. $\left[Z_{real_{flex}}, Z_{img_{flex}}\right]$*:* real and imaginary parts of the inflection point in the MF semicircle.
13. $\left[Z_{real_{Knee}}, Z_{img_{Knee}}\right]$*:* real and imaginary parts of the knee point separating the LF and MF regions.
14. $Z_{img_{Max}}$: max value of the imaginary component.
15. $Z_{img_{Min}}$: minimum value of the imaginary component.
16. $Z_{real_{Max}}$*:* max value of the real component.

A visual representation of the extracted features on a Nyquist plot is provided in Figure 3.

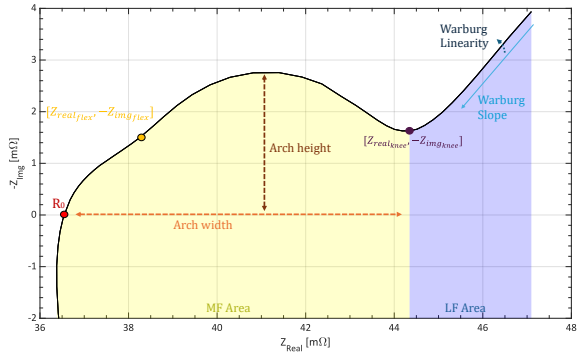

Figure 3. Main features extracted from the Nyquist Diagram

2.2. Data Preparation and Feature Evaluation

To properly execute the processing steps of the proposed pipeline, the extracted features are first normalized setting their initial value equal to 1. This process ensure that the evaluation procedure is not influenced by the different scales of the considered quantities. Specifically, to prevent the normalization from being affected by potentially unstable initial values, each feature is normalized using the average initial value of the first 10 cycles. Since the cells are tested in stressful operating conditions, considering more cycles could introduce biases due to early degradation. In addition, to smooth the feature trends, the data are filtered using an Exponentially Weighted Moving Average (EWMA) filter, as specified in the following:

$$\tilde{f}_j(k) = \alpha \cdot f_j(i) + (1-\alpha)\cdot \tilde{f}_j(i-1), \qquad j = 2{:}N_f \qquad (1)$$

where α is the smoothing factor, experimentally set to 0.2, N_f is the number of features; and f_j and $\tilde{f}_j$ represent the j-th feature before and after filtering, respectively. It is worth noting that α has been set to balance smoothing with trend responsiveness. This conditioning phase is applied to reduce feature noise, thereby improving the quality of the final HI.

Figure 4 shows the trends of the preprocessed features for a representative cell. As can be observed, the curves exhibit generally monotonic trends, although their evolution differs depending on the physical parameter considered. In particular, peaks and drops may appear at different cycle numbers according to the underlying electrochemical phenomenon. It is worth noting that the filtering stage is not intended to completely smooth the feature trends. For this reason, a quantitative metric is introduced to evaluate the roughness of each derived feature. The roughness is computed as the mean local variation between consecutive feature values, normalized by the overall feature range. The corresponding expression is:

$$R = \frac{\sum_{i=1}^{N-1} \left|\tilde{f}_{J_{i+1}} - \tilde{f}_{J_i}\right|}{(N-1)\left(\tilde{f}_{J_{Max}} - \tilde{f}_{J_{min}}\right)} \qquad (2)$$

where N is the number of samples of the considered feature.

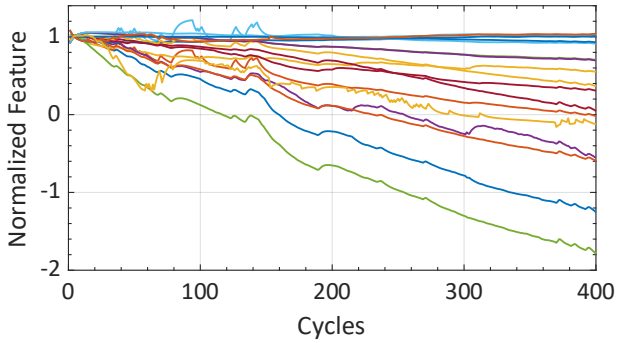

Figure 4. Preprocessed features for a randomly selected cell.

To assess the quality of each feature and its potential usefulness for diagnostic purposes, a score based on the Spearman correlation between the feature trend and a reference degradation model is assigned.

The adopted reference model is a single-exponential function, which has been shown to effectively describe the degradation behavior of electrochemical cells (Catelani et al., 2021), defined as follows:

$$C(i) = C_0 + a \cdot \exp(b/i) \tag{3}$$

where C_0 represents the rated capacity, and a and b are coefficients describing the degradation dynamics.

The overall score accounts not only for the similarity between the feature trend and the expected capacity decay, but also for the stability of the feature curve in view of generating a reliable HI output. Using the previously defined roughness metric, noisy features are penalized. As expressed in Equation (4), the score of each feature is weighted by a $(1 - kR)$ factor, where k is a properly tuned coefficient. In the analyses reported in Section 4, k is set to 20.

$$score_j = (1 - k \cdot R) \cdot corr(\tilde{f}_j, mdl_{(3)}) \tag{4}$$

This strategy enables prioritization of the most stable features among those exhibiting the highest prognostic relevance.

2.3. HI extraction

Once the features and their corresponding scores are available, it is necessary to define a strategy to combine them into a single Health Indicator (HI) that preserves the relevant information and effectively reflects the battery health condition. In this work, an exponential-based weight attribution algorithm is adopted, as reported in Equation (5):

$$\begin{cases} w_{\tilde{f}_j} = e^{\left(1 - \frac{1}{\frac{1}{(1-th)} \cdot (score_j - th)}\right)}, & for\ score_j > th \\ w_{\tilde{f}_j} = 0, & for\ score_j \le th \end{cases} \tag{5}$$

This formulation assigns weights within the interval $[0, 1]$, distributing their values so as to strongly emphasize features with higher scores while suppressing low-quality ones.

The acceptance threshold th is experimentally set to 0.6 to prevent the contribution from being concentrated on only a few parameters. Further validation of this choice is discussed later in the paper.

A preliminary "raw" health indicator is then obtained by linearly combining the weighted features:

$$HI = \frac{\sum_1^{N_f} \tilde{f}_j \cdot w_{\tilde{f}_j}}{\sum_1^{N_f} w_{\tilde{f}_j}} \tag{6}$$

The normalization by the total weight sum ensures that the HI starts from a unitary initial value and remains properly scaled. However, not all impedance variations evolve synchronously with cycle aging, and delays between different physical phenomena may occur. As a result, the aggregated HI trend may overestimate or underestimate the actual capacity degradation, particularly in the mid-life region of the battery. To enhance the stability of the HI over the entire lifespan, a regularization term is introduced once a sufficient number of feature samples has been collected. Specifically, the first n samples of the HI are fitted using the degradation model defined in Equation (3) to estimate a reference exponential trend. In the developed method the regularization is activated after 80 cycles. The final HI is then adjusted according to:

$$\widehat{HI} = (1 - \lambda) \cdot HI + \lambda \cdot fit(HI(1{:}n),\ mdl_{(3)}) \tag{7}$$

Where λ is a coefficient that controls the strength of the reference fitted curve in shaping the final HI trend. It is important to emphasize that the purpose of this regularization is not to enforce the degradation model, but rather to reinforce the expected exponential behavior of the HI while preserving its data-driven nature. The validation and tuning of the adopted coefficients are discussed in the following sections

3. DATASET

3.1. Data Acquisition

To validate the proposed framework, a custom lithium-ion battery dataset was developed. Specifically, six cylindrical 18650 Nickel–Manganese–Cobalt (NMC) cells with a rated capacity of 2.5 Ah were tested under an accelerated life testing campaign.

The devices under test (DUTs) were charged using a Constant-Current Constant-Voltage (CCCV) protocol with a charging current of 4 A (corresponding to a 1.6C rate), a maximum charge voltage of 4.2 V, and a cut-off current of 0.2 A during the CV phase. Discharge was performed at a constant current of 10 A (i.e., 4C) until the lower voltage threshold of 2.5 V was reached. After each charge and discharge phase, the cells were left in an idle state for 30 minutes to allow stabilization of the internal electrochemical

processes. EIS measurements were conducted at the end of the post-charge rest period.

At each cycle, EIS was performed by applying a potentiostatic sinusoidal excitation signal over a frequency range from 50 mHz to 50 kHz, acquiring 10 logarithmically spaced frequency points per decade. The experimental campaign lasted 400 cycles, during which all tested cells reached a SOH level below 80% (i.e., the typical failure threshold condition in automotive application).

3.2. Test Equipment

The experimental campaign was carried out using a dedicated battery testing setup composed of an Arbin battery tester, a safety datalogger, and a Gamry Interface 5000E for Electrochemical Impedance Spectroscopy (EIS) measurements. More specifically, the Arbin LBT is a bidirectional power supply capable of simultaneously charging and discharging multiple cells, supporting up to 16 independent channels. Each channel operates with current and voltage limits of 30 A and 5 V, respectively. The system enables data acquisition with a sampling rate up to 2 kSa/s and 24-bit resolution. The battery tester is directly interfaced with a safety datalogger, which monitors potential battery overheating through thermocouples, as well as with the EIS instrument via a dedicated testing suite installed on a PC workstation.

The Gamry Interface 5000E is directly connected with the battery test equipment, allowing impedance measurements over a wide frequency range for all the tested units. A temperature chamber is also used to host the batteries during the experimental campaign setting the operating conditions during the tests. A picture of the entire experimental platform is reported in Fig. 5.

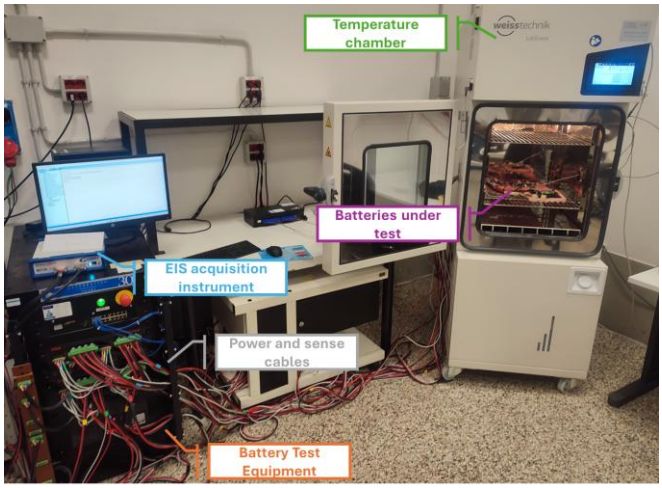

Figure 5. Complete experimental platform used to acquire the required dataset.

4. EXPERIMENTAL RESULTS AND DISCUSSION

4.1. Performance of the HI

To assess the performance of the proposed strategy, the resulting HIs are compared with the traditional SOH definition based on discharge capacity, as shown in Figure 6. From these plots, a strong agreement between the proposed HIs and the actual SOH levels can be observed, with an almost complete overlap for Cell #1 and Cell #6, as well as very good performance for all the other cells. This result provides a preliminary confirmation of the effectiveness of the proposed approach, demonstrating that the HI trends accurately reproduce the battery degradation behavior.

To enable a direct comparison with existing HI extraction approaches, a traditional framework based on PCA is adopted as a reference method to reduce the dimensionality of the feature set and derive a single HI. Specifically, the reference approach ranks the features according to their score, selects the best eight, and computes the HI from this reduced subset. For quantitative evaluation, the Root Mean Square Error (RMSE) and the coefficient of determination (R^2) between the estimated HIs and the ground-truth SOH values are computed for both the proposed approach and the PCA-based state-of-the-art approach. The considered metrics provide a statistical assessment of the accuracy and goodness of fit of the estimated HI trajectories with respect to the actual SOH degradation trend. Furthermore, the Maximum Absolute Error (MaxAE) is also computed to evaluate the worst-case deviation between the estimated HI and the ground-truth SOH. The comparative results are collected in Table 1, which reports the RMSE, R^2 and MaxAE values obtained with each method. The R^2 results obtained with the proposed HI indicate excellent performance in terms of trend shape, with values exceeding 0.94 for all the analyzed cells.

In contrast, the PCA-based approach shows significant cell-to-cell variation in this value, indicating low adaptability. Moreover, the proposed HI consistently achieves lower RMSE and MaxAE values than the PCA-based HI. The most significant improvements are observed for Cell #1 and Cell #6, where the RMSE reduction reaches 74.40% and 73.27%, respectively. Similarly, the reduction of the MaxAE indicates that the HI is reliable along all the battery lifespan. This aspect is particularly relevant for automotive applications, where accurate SOH assessment must be ensured over the entire operating period.

Additionally, Figure 7 shows the corresponding HI curves obtained with the proposed and PCA-based methods alongside the HI obtained from the single best feature and the ground-truth SOH profile, enabling a visual comparison of their ability to capture the underlying degradation behavior. It can be noticed that, although the single best feature approach performs better than the PCA for the units shown, it gives worse and more unstable results with respect to the presented algorithm.

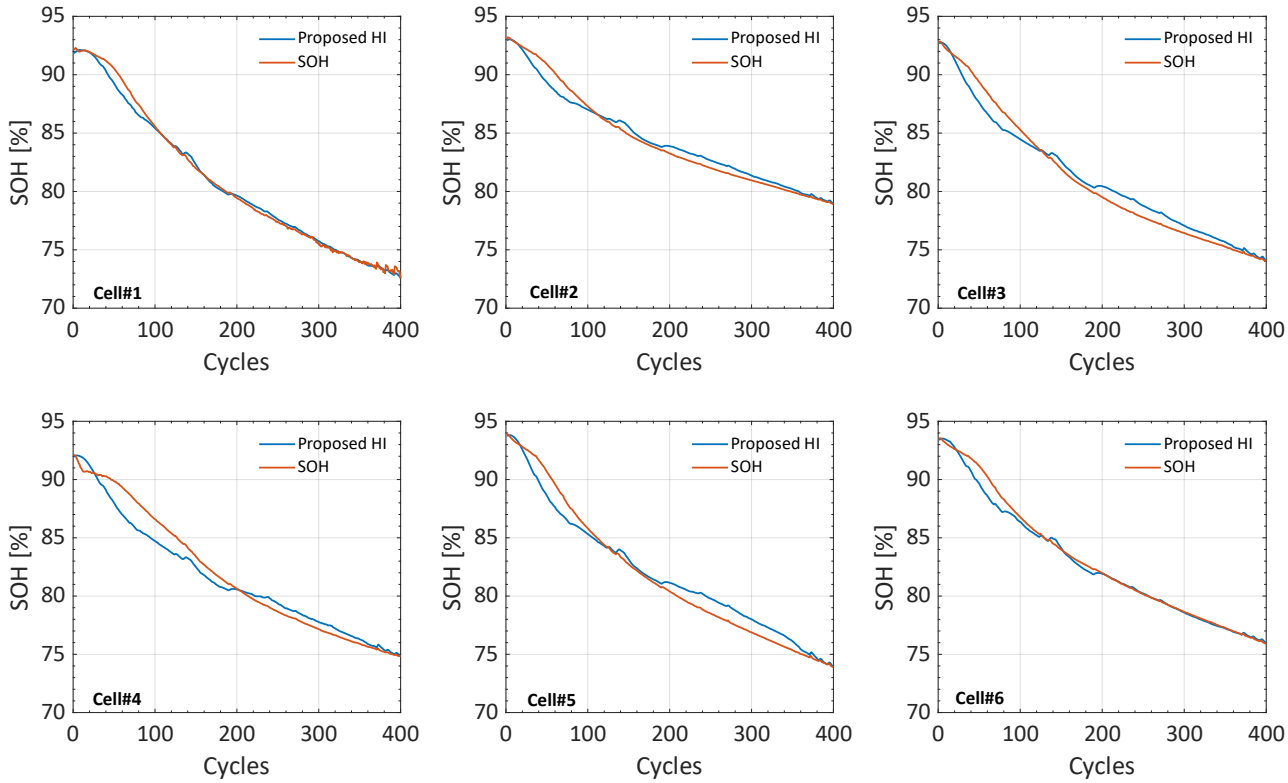

Figure 6. Comparison with proposed HI and actual SOH derived from the discharge capacity

Table 1. RMSE, R^2 and Max AE values of the proposed method compared to an alternative PCA-based method

Cell ID	PCA-based HI			Proposed HI		
	RMSE [SOH %]	R^2	MaxAE [SOH%]	RMSE [SOH %]	R^2	MaxAE [SOH%]
#1	1.724	0.912	3.378	0.441	0.994	1.386
#2	2.222	0.749	3.991	0.644	0.971	1.587
#3	2.269	0.837	4.159	0.882	0.968	1.820
#4	2.150	0.822	3.841	1.092	0.946	2.458
#5	2.873	0.762	4.415	0.985	0.963	2.143
#6	2.008	0.870	4.020	0.537	0.988	1.709

Furthermore, in terms of computational burden the developed method results to be slightly faster than traditional PCA-based technique with approximately equal peak memory usage. More in detail, in Table 2, the execution time and the peak memory usage of the 2 implemented functions are shown as average value and standard deviation of 30 repeated runs implemented on MATLAB 2024b by using a PC workstation equipped with Intel Core i9-12900K CPU and 32 GB RAM.

These results demonstrate superior performance of the proposed framework compared with the PCA-based approach also in terms of computational burden.

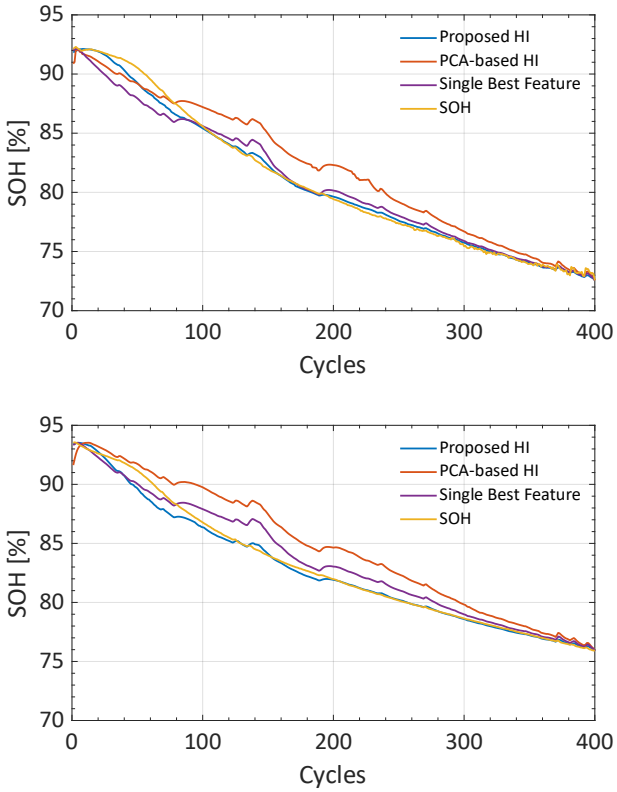

Figure 7. Comparison with proposed HI and a PCA-based approach with respect to the actual SOH

Table 2. Run time and Memory peak usage of the proposed method compared to an alternative PCA-based method

Method	Run Time [ms]	Memory Peak [MB]
PCA-based	94.7 ± 7.8	0.24
Proposed	67.7 ± 3.9	0.25

4.2. Contribution of the selected features

One of the most critical aspects of combined Health Indicators lies in the limited transparency regarding how the selected physical parameters contribute to the construction of the final HI. In the developed framework, a preliminary validation of the overall relevance of the adopted features can be obtained by analyzing their average scores across the examined batteries.

Figure 8 presents the bar chart of the mean scores and corresponding weights computed across all tested cells. Most features exhibit average score values above the 0.6 acceptance threshold, confirming their effectiveness in contributing to the HI formulation. Conversely, the ohmic resistance and certain instantaneous parameters, such as $Z_{img_{Max}}$ and $Z_{real_{flex}}$, show average scores significantly below the threshold.

By examining the average weights shown in the figure, it can be observed that the proposed weighting strategy adaptively adjusts the contribution of each feature on a cell-by-cell basis, leading to heterogeneous weight distributions among the selected parameters. It is worth noting how *R0* exhibit a poor overall score, thereby proving its high sensitivity to the operating conditions and its unreliability as a stand-alone HI.

Nevertheless, even features with lower average rankings contribute meaningfully to at least one of the tested cells. This behavior supports the rationale behind the adopted feature set and highlights the flexibility of the proposed scoring and weighting mechanism.

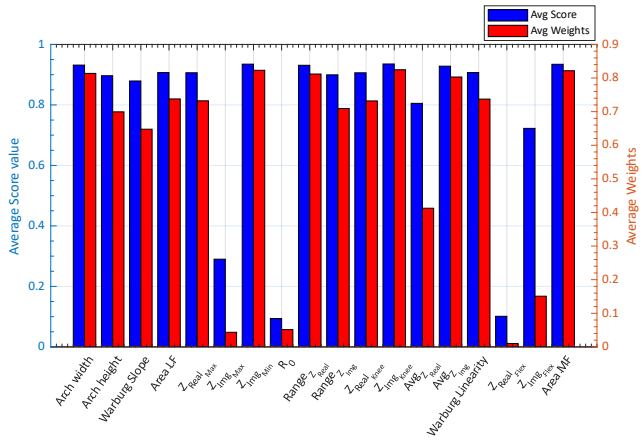

Figure 8. Average score and weight of each feature

4.3. Validation by varying input parameters

An additional key step in validating the presented strategy consists in analyzing the impact of the input coefficients adopted at different stages of the processing chain. This assessment provides transparent insight into the methodology, supporting its repeatability and potential generalizability to different energy storage devices. The first analysis concerns the selection of the coefficient k, which controls the penalization of feature roughness during the score assignment process.

The average of the RMSE obtained across all cells by varying k are reported in Table 3. Increasing k from 10 to 20 results in an improvement of the mean RMSE by 4.49%. However, further increases significantly degrade the HI performance, as excessive roughness penalization suppresses features that are still informative for health monitoring.

The robustness of the weight assignment algorithm defined in Section 2.3 is further assessed by analyzing the effect of varying the threshold parameter. A Monte Carlo sensitivity analysis is performed by randomly perturbing the threshold value within a ±20% interval around the nominal value, assuming a uniform distribution. The simulation consists of 10,000 iterations, enabling evaluation of result stability under conservative perturbation conditions. For brevity, the sensitivity results for a representative cell are shown in Figure 9. The resulting HI trends exhibit only minor variations, with a maximum deviation limited to 0.25% of the SOH in the intermediate portion of the battery lifespan. These findings demonstrate the robustness of the developed framework with respect to variations in the weight assignment threshold.

Table 3. Mean RMSE with different roughness coefficients

ROUGHNESS COEFFICIENT k	MEAN RMSE [SOH %]
10	0.799
20	0.764
30	0.850
40	1.044

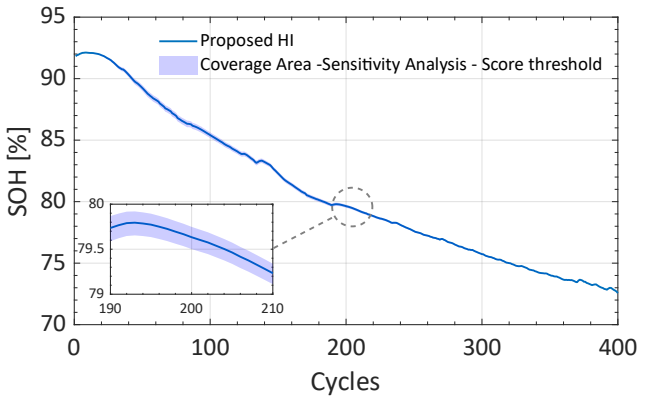

Figure 9. Sensitivity analysis of the score threshold on the proposed framework for HI development.

Finally, the impact of the regularization stage is analyzed. Specifically, the effect of varying the regularization coefficient λ is evaluated. Table 4 reports the RMSE, R^2 and MaxAE values obtained by varying λ between 0.5 and 0.8, all averaged across the six batteries. Despite a slightly higher mean value of the MaxAE, the best performances are achieved for $\lambda = 0.7$, with significantly lower RMSE and R^2 averaged values. Nevertheless, the health assessment does not significantly deteriorate within the tested range, as indicated by the similar goodness-of-fit values with respect to the actual SOH trend.

Additionally, the number of initial cycles required to derive a stable reference model for regularization is investigated. Table 5 reports the mean values across all batteries of RMSE, R^2 and MaxAE metrics obtained when fitting the correction model at different battery life stages. As expected, increasing the number of cycles used to estimate the reference model improves the SOH estimation.

However, these improvements progressively diminish as more cycle data become available. This analysis indicates that using the first 80 cycles to derive the reference model provides an optimal balance. Including additional cycles does not further enhance monitoring accuracy and may introduce instability in the guiding model, potentially degrading overall performance.

Overall, the results in terms of R^2 confirm that the HI output can be considered reliable after at least the first 40 cycles are available.

Table 4. Mean RMSE, R^2 and Max AE at different λ values

REGULARIZATION TERM λ	MEAN RMSE [SOH %]	MEAN R^2	Mean MaxAE [SOH%]
0.5	1.245	0.933	2.313
0.6	0.930	0.960	1.724
0.7	0.764	0.972	1.850
0.8	1.053	0.949	2.437

Table 5. Mean RMSE, R^2 and Max AE by fitting the reference model after different number of cycles

INITIAL CYCLES	MEAN RMSE [SOH %]	MEAN R^2	Mean MaxAE [SOH%]
20	1.411	0.919	2.513
40	0.953	0.955	2.000
60	0.783	0.968	1.835
80	0.764	0.972	1.850
100	0.849	0.966	2.059

5. CONCLUSION

This paper presented an innovative framework for extracting a single Health Indicator (HI) for battery SOH assessment directly from EIS measurements. By introducing a reference degradation model, the proposed approach demonstrates promising results in improving the accuracy of the derived HIs in tracking the actual capacity fading caused by cycle aging. Moreover, the proposed framework is characterized by a transparent and computationally efficient structure, making it suitable for feasible implementation in real-time on-board system within the vehicle.

This approach have been validated on high stress conditions for a homogeneous set of batteries, yet future research will further include a wider range of operating conditions and different energy storage technologies. Such extended evaluations will allow assessment of the robustness and scalability of the approach, ultimately supporting its generalization to diverse electric vehicle applications.

ACKNOWLEDGEMENT

This work was developed within the framework of the project "ModEling And SimUlation of gREen hydrogen Systems FOR P2X (MEASURES FOR P2X)" code P2022ZT2LC (CUP D53D23016230001) supported by the Italian project PRIN 2022 PNRR receiving funding from the European Union Next-GenerationEU (PIANO NAZIONALE DI RIPRESA E RESILIENZA (PNRR) – MISSIONE 4 COMPONENTE 2, INVESTIMENTO 1.1 – D.D. 1181 27/07/2023. This manuscript reflects only the authors' views and opinions; neither the European Union nor the European Commission can be considered responsible for them.

REFERENCES

Bian, J., Liu, G., Chen, J., Cao, Y., Chen, R., & Qian, Y. (2025). PSO-MLSt-LSTM: Multi-layer stacked ensemble model for lithium-ion battery SOH prediction via multi-feature fusion. *Journal of Energy Storage*, *125*, 116825. https://doi.org/10.1016/j.est.2025.116825

Catelani, M., Ciani, L., Fantacci, R., Patrizi, G., & Picano, B. (2021). Remaining Useful Life Estimation for Prognostics of Lithium-Ion Batteries Based on Recurrent Neural Network. *IEEE Transactions on Instrumentation and Measurement*, *70*, 1–11. https://doi.org/10.1109/TIM.2021.3111009

Dini, P., Colicelli, A., & Saponara, S. (2024). Review on Modeling and SOC/SOH Estimation of Batteries for Automotive Applications. *Batteries*, *10*(1), 34. https://doi.org/10.3390/batteries10010034

Dong, M., Li, X., Yang, Z., Chang, Y., Liu, W., Luo, Y., Lei, W., Ren, M., & Zhang, C. (2024). State of health

(SOH) assessment for LIBs based on characteristic electrochemical impedance. *Journal of Power Sources*, *603*, 234386. https://doi.org/10.1016/j.jpowsour.2024.234386

Du, X., Meng, J., Amirat, Y., Gao, F., & Benbouzid, M. (2025). Feature selection strategy optimization for lithium-ion battery state of health estimation under impedance uncertainties. *Journal of Energy Chemistry*, *101*, 87–98. https://doi.org/10.1016/j.jechem.2024.09.032

Guo, A. Y., Hou, B. R., Li, C. P., & Xu, D. L. (2024). EIS Based ECM Parameter and SOH Estimation for LiFePO $_4$ Battery Considering SOC Effect. *2024 IEEE 10th International Power Electronics and Motion Control Conference (IPEMC2024-ECCE Asia)*, 3362–3368. https://doi.org/10.1109/IPEMC-ECCEAsia60879.2024.10567445

Iurilli, P., Brivio, C., & Wood, V. (2021). On the use of electrochemical impedance spectroscopy to characterize and model the aging phenomena of lithium-ion batteries: a critical review. *Journal of Power Sources*, *505*, 229860. https://doi.org/10.1016/j.jpowsour.2021.229860

Lee, H., Yoo, M. Y., Choi, J.-H., Sung, W., & Heo, J. S. (2024). State-of-Charge and State-of-Health Estimation for Li-Ion Batteries of Hybrid Electric Vehicles under Deep Degradation. *PHM Society European Conference*, *8*(1), 10. https://doi.org/10.36001/phme.2024.v8i1.4032

Omakor, J., Miah, M. S., & Chaoui, H. (2024). Battery Reliability Assessment in Electric Vehicles: A State-of-the-Art. *IEEE Access*, *12*, 77903–77931. https://doi.org/10.1109/ACCESS.2024.3406424

Patrizi, G., Canzanella, F., & Ciani, L. (2025). Towards a Novel Indirect Battery Health Indicator Based on Electrochemical Impedance Spectroscopy for RUL Estimation in Electric Vehicles. *2025 IEEE International Workshop on Metrology for Automotive (MetroAutomotive)*, 139–144. https://doi.org/10.1109/MetroAutomotive64646.2025.11119269

Shan, R., Wang, Y., Guo, S., Cui, Y., Zhao, L., Li, J., & Wang, Z. (2025). From Empirical Measurements to AI Fusion—A Holistic Review of SOH Estimation Techniques for Lithium-Ion Batteries in Electric and Hybrid Vehicles. *Energies*, *18*(13), 3542. https://doi.org/10.3390/en18133542

Yang, S., Zhang, C., Jiang, J., Zhang, W., Zhang, L., & Wang, Y. (2021). Review on state-of-health of lithium-ion batteries: Characterizations, estimations and applications. *Journal of Cleaner Production*, *314*, 128015. https://doi.org/10.1016/j.jclepro.2021.128015

Yu, J., Guo, Y., & Zhang, W. (2024). Anomaly Detection for Charging Voltage Profiles in Battery Cells in an Energy Storage Station Based on Robust Principal Component Analysis. *Applied Sciences*, *14*(17), 7552. https://doi.org/10.3390/app14177552

Zhou, Z., Li, Y., Wang, Q.-G., & Yu, J. (2023). Health Indicators Identification of Lithium-Ion Battery From Electrochemical Impedance Spectroscopy Using Geometric Analysis. *IEEE Transactions on Instrumentation and Measurement*, *72*, 1–9. https://doi.org/10.1109/TIM.2023.3272401